# Lab on a Chip

Accepted Manuscript


Resonant microbubbles are sorted from a polydisperse ultrasound contrast agent suspension in an acoustic bubble sorting chip.

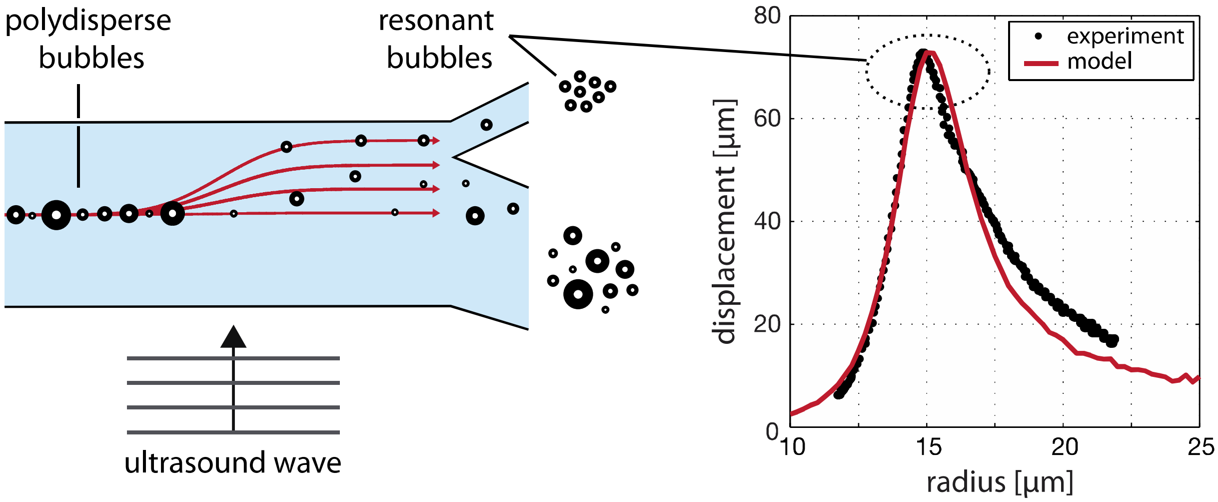

# Acoustic bubble sorting for ultrasound contrast agent enrichment

**Tim Segers,[*a] and Michel Versluis[a]**

***Received Xth XXXXXXXXXX 20XX, Accepted Xth XXXXXXXXX 20XX***
***First published on the web Xth XXXXXXXXXX 200X***
**DOI: 10.1039/b000000x**

An ultrasound contrast agent (UCA) suspension contains encapsulated microbubbles with a wide size distribution, with radii ranging from 1 to 10 $\mu$m. Medical transducers typically operate at a single frequency, therefore only a small selection of bubbles will resonate to the driving ultrasound pulse. Thus, the sensitivity can be improved by narrowing down the size distribution. Here, we present a simple lab-on-a-chip method to sort the population of microbubbles on-chip using a traveling ultrasound wave. First, we explore the physical parameter space of acoustic bubble sorting using well-defined bubble sizes formed in a flow-focusing device, then we demonstrate successful acoustic sorting of a commercial UCA. This novel sorting strategy may lead to an overall improvement of the sensitivity of contrast ultrasound by more than 10 dB.

## 1 Introduction

Ultrasound is the most widely used medical imaging modality. It is based on the scattering of acoustic waves from inhomogeneities in tissue. Blood, however, is a poor ultrasound scatterer and the visibility of the blood pool can be enhanced using stabilized microbubbles as an ultrasound contrast agent (UCA). The bubbles produce a strong resonant echo, which can be 1 billion times stronger than the echo of solid particles of the same size[1], owing to the large compressibility of the gas core of the bubbles. The contrast enhancement makes it possible to visualize the blood pool and to quantify organ perfusion[2]. The sensitivity of bubble detection down to single bubbles *in-vivo* facilitates targeted molecular imaging applications using ultrasound with targeting ligands attached to the bubble shell[3]. UCAs can also be loaded with drugs, e.g. for the local delivery of chemotherapeutic drugs with a narrow therapeutic index[4,5], or genes, such as siRNAs[6,7].

The oscillation of the bubbles in the driving ultrasound field is governed by a strong coupling between the microbubble size and the ultrasound driving frequency through the Minnaert eigenfrequency of the bubbles[8]. UCAs are commercially available as a suspension of encapsulated microbubbles with a relatively wide manufacturer-dependent size distribution with radii ranging from 1 to 10 $\mu$m. Clinical ultrasound systems operate at a narrow bandwidth optimized for the type of ultrasound transducer and clinical application, consequently only a small fraction of the bubbles resonates to the driving ultrasound field. Thus, the sensitivity of contrast-enhanced ultrasound perfusion imaging can be improved by narrowing down the size distribution. Moreover, a fully resonant bubble population of drug-loaded agents will be much more efficient in the local delivery to target cells, in addition to saving a substantial portion of its expensive or toxic payload. For preclinical testing in small animal models, the injected contrast agent volume is much lower than the volume that can be injected into humans, so also here one could benefit from enriched, more resonant, contrast bubbles. Finally, for the use of targeted molecular imaging with ultrasound it would be highly beneficial to discriminate adherent bubbles from freely floating ones, which can be achieved through spectral differences through a resonance shift of the adherent bubbles of a single size[9,10]. Moreover, only a small percentage of the total injected dose is typically retained at the target site and it is therefore important to have all of the targeted bubbles in the size range optimized for detection. For all these reasons it is of great interest to devise a method to inject only the resonant bubbles.

A resonant bubble suspension can be realized in three different ways: monodisperse bubbles can be formed directly in a flow-focusing device, or commercially available UCA can be filtered or they can be sorted. Flow-focusing techniques have proven to be a versatile tool for highly controlled formation of monodisperse droplets and bubbles[11,12]. In a flow-focusing geometry a gas thread is focused in between two external liquid flows through a constriction, where the gas is pinched off to form monodisperse bubbles[13,14]. One challenging aspect of this approach is to investigate how the monodisperse bubbles could be encapsulated with a biocompatible coating to stabilize them[15–17], to investigate how to maintain the monodispersity of bubbles produced at high production rates over time[18], and to investigate the dynamics of different coating materials for in-vivo and clinical use[19]. Enriching commercially avail-

† Electronic Supplementary Information (ESI) available: [details of any supplementary information available should be included here]. See DOI: 10.1039/b000000x/

*Physics of Fluids Group and MESA+ Institute of Nanotechnology, P.O. Box 217, 7500 AE Enschede, The Netherlands. Fax: +31 53 489 8068; Tel: +31 53 489 2470; E-mail: t.j.segers@utwente.nl*

able UCAs can be done by means of mechanical filtration[20]. Bubbles can be filtered by a pore filter, however, this may easily result in bubble fragmentation due to elevated pressures and to filter clogging. Moreover, bubbles not passing the filter are lost and can not be re-used.

Size-selective sorting methods are based on the forcing of bubbles. Bubbles with a different size experience a body force of different magnitude. The force can be a result of gravity, fluidic forces, or radiation forces, both optical and acoustical. One sorting method is reported by Goertz *et al.*[21] who isolated smaller bubbles through decantation. The basis of this procedure is that gravitational forces are balanced by viscous drag forces; larger bubbles rise faster in the fluid due to a larger buoyant force although in practice this is not a well-controlled process. Similarly, Feshitan *et al.*[22] isolate size fractions from a polydisperse UCA by centrifuging the suspension. A cylinder with the agent is rotated at high speed after which the bubbles were extracted from the cylinder at certain heights.

On-line continuous sorting methods for bubbles are not reported to the best of our knowledge. However, numerous publications on microfluidic continuous sorting methods for particles and cells are presented. Nieuwstadt *et al.*[23] use lift forces to sort particles in a straight microfluidic channel. Another method to sort particles in a flow field is called pinched flow fractionation, first reported by Yamada *et al.*[24]. Sorting particles in acoustic fields is extensively reported[25–28]. In general, an ultrasound standing wave (USW) is set up between two reflecting channel walls in a $\lambda/2$ microfluidic resonator chip resulting in a pressure node in the center of the channel. Particles are injected into the channel from where they will be dispersed over the width of the channel by the primary radiation force. While solid particles are mainly driven by the primary radiation force of the ultrasound, bubbles will also be susceptible to radiation pressure generated by neighbouring bubbles, termed secondary radiation force[29,30]. Moreover, the reflecting walls present the bubbles with a virtual image bubble which through the secondary radiation force leads to mutual attraction, illustratively named the Narcissus effect[31]. Primary and secondary radiation forces for bubbles are of the same order of magnitude making an USW sorting strategy unfeasible through bubble clustering and drift towards the channel walls.

The use of a *traveling* acoustic wave has the advantage that the channel dimensions are decoupled from the wavelength of the ultrasound. Therefore the frequency can be tuned for optimal performance in the required size range of the sorting chip. Here, we present a new and simple acoustic bubble sorting method contained in a lab-on-a-chip device. We make use of travelling waves of low acoustic pressure. The use of continuous wave ultrasound allows for a finite net displacement of the bubbles during multiple cycles, whereas the ultrasound frequency allows for size-selectivity through resonance. First we describe the design of the microfluidic device in which the bubbles can be sorted. We test its working principle for bubbles of well-defined size formed in a flow-focusing device and show that sorting bubbles with a size similar to those contained in UCAs is feasible. Finally, we show that a suspension of UCA bubbles can be efficiently sorted using this novel sorting strategy.

## 2 Acoustic bubble sorting theory

A traveling ultrasound wave propagates in positive $y$-direction (the vertical in Fig. 1):

$$P(y,t) = P_A \sin(2\pi f t - ky), \tag{1}$$

where $k = 2\pi f/c$ is the wavenumber of the wave with frequency $f$ and speed of sound $c$ and with $P_A$ the acoustic pressure amplitude. A bubble will experience a radiation force

$$F_R = -V \cdot \nabla P, \tag{2}$$

where both the pressure gradient $\nabla P$ and the volume $V$ of the bubble are time-dependent with different phase contributions. This leads to an unsteady force that changes periodically both in direction and in magnitude[32].

The time dependent volume of the bubble in the traveling wave can be obtained from a Rayleigh-Plesset-type equation[32]:

$$\rho\left(\ddot{R}R + \frac{3}{2}\dot{R}^2\right) = \left(P_0 + \frac{2\sigma}{R_0}\right)\left(\frac{R_0}{R}\right)^{3\kappa}\left(1 - \frac{3\kappa\dot{R}}{c}\right) - P_0 - P_A - \frac{2\sigma}{R} - \frac{4\nu\dot{R}}{R}, \tag{3}$$

where $\rho$ is the liquid density, $c$ the speed of sound in the liquid, $\kappa$ the polytropic exponent of the gas inside the bubble, with $P_0$ the local hydrodynamic pressure within the channel and $P_A$ the acoustic pressure, as before. $R_0$ is the initial bubble radius, $R$ the time-dependent radius of the bubble and the overdots denote its time derivatives. The solution to Eq. (3) gives the radius of the bubble as a function of time, $R(t)$.

The translational motion of a bubble in the y-direction propelled by the primary radiation force $F_R$ is counteracted by a viscous drag force $F_D$ and due to acceleration of the bubble by an added mass force $F_A$[33–35]. UCA bubbles are coated with phospholipids that fully immobilize the gas-air interface and they can therefore be modeled using a point-particle approach as rigid spheres with a time dependent radius. We set up the force balance for this system:

$$0 = F_R + F_A + F_D = \frac{4}{3}\pi R^3 \dot{u}_l \rho - \frac{1}{2}\rho_l \frac{d}{dt}\left(\frac{4}{3}\pi R^3(\dot{y}_b - u_l)\right) - 6\pi\mu R(\dot{y}_b - u_l), \tag{4}$$

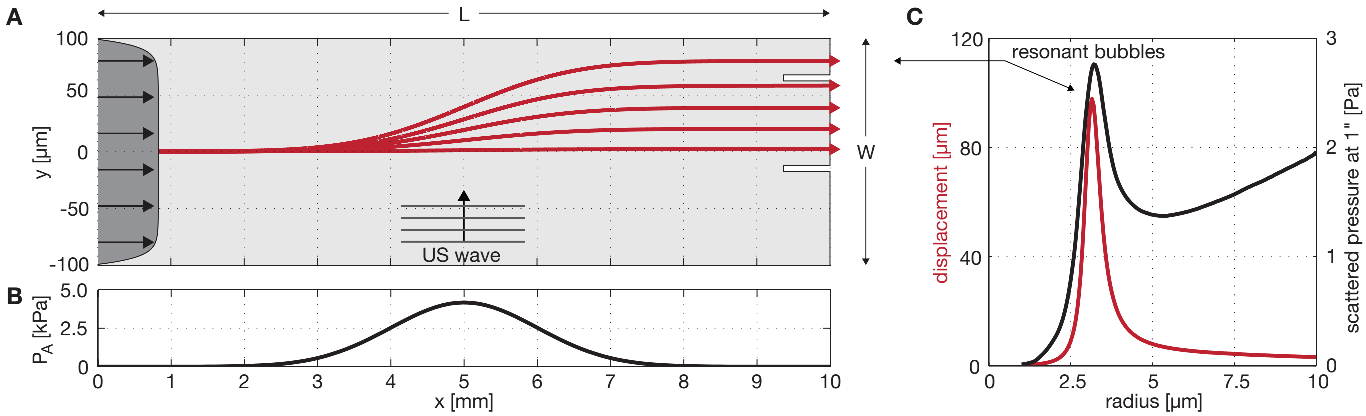


**Fig. 1** The acoustic bubble sorting principle. (A) Bubble trajectories in a high aspect ratio microfluidic channel (L = 1 cm, W = 200 $\mu$m, $W/H$ = 10). Size-selectivity is accomplished through the resonant behavior of the microbubbles by the radiation force of a traveling acoustic wave with a maximum pressure amplitude of 4.5 kPa (B). Figure C shows the displacement (red solid line) from the center of the channel (y = 0) as a function of the bubble radius. The black solid line in C shows the scattered pressure calculated at a distance of 1 in. as a function of the bubble size. The resonant bubbles are displaced over the largest distance into the upper outlet and are therefore separated from the polydisperse bubble population. The pressure scattered from the resonant bubbles is the largest as can be seen from the black line in figure C.

where $\dot{y}_b$ is the transverse velocity of the bubble, $u_l$ is the fluid velocity and $d/dt$ represents differentiation with respect to time. Inertia of the bubble is neglected because of the small gas density as compared to water.

The radiation force $F_R$ on a bubble due to the pressure wave is calculated from the pressure gradient $\partial P/\partial x = -\rho Du/Dt$. Convective effects are negligible here and it reduces to $\partial P/\partial x = -\rho_l \partial u_l/\partial t$ [36]. The added mass force $F_A$ gives the force that must be exerted in order to accelerate a rigid sphere in its surrounding fluid, and for spherical objects it is well-known[37]. It is independent of the boundary condition and of the Reynolds number, however since $R$ and $u_l$ are time-dependent, the expression for the added mass force is more extended: $F_A = 2/3\pi\rho R^3(\dot{u}_l - \ddot{y}_b) + 2\pi\rho R^2\dot{R}(u_l - \dot{y}_b)$. The quasi-steady drag $F_D$ describes the Stokes drag acting on the bubbles as they are translated. Simple Stokes drag was taken because the bubbles are insonified at low acoustic pressures ($P_A \approx 10$ kPa) resulting in relatively small translational velocities $\dot{y}_b$ and bubble Reynolds numbers ($Re_b = 2\rho R\dot{y}_b/\mu$) smaller than 1. The laminar flow field $u$ in a microchannel with a rectangular cross-section at a given lateral position $y$ and a height level $z$ can be calculated by solving the Hagen-Poiseuille equation, see e.g. Bruus[38]:

$$u(y,z) = \frac{4H^2\Delta P}{\pi^3\mu L}\sum_{n,odd}^{\infty}\frac{1}{n^3}\left[1 - \frac{cosh(n\pi\frac{y}{H})}{cosh(n\pi\frac{W}{2H})}\right]\sin(n\pi\frac{z}{H}), \quad (5)$$

with $L$ the length of the channel, $W$ its width and $H$ its height, $\mu$ the kinematic viscosity of the liquid and $\Delta P$ the pressure drop across the channel. For a channel with an aspect ratio $W/H$ of 10 the flow profile is shown entering from the left in Fig. 1A. Thus, lift forces, which may counteract the translation induced by the ultrasound, are negligible because of the absence of a flow gradient (hence zero vorticity) over almost the entire channel width $W$.

The translation of bubbles in a size range of 1 to 10 $\mu$m transported by flow with a maximum downstream velocity of 0.1 m/s through a microfluidic channel is modeled by solving the coupled radial dynamics, Eq. (3) and translation, Eq. (4). As a first approximation, we assume that the microfluidic channel is acoustically transparent. This implies that the bubbles do not interact with the channel walls. Furthermore, it is assumed that the bubbles are initially positioned at the center of the channel (both in width and in height, $y = 0; z = 0$) and that they are transported downstream with the flow velocity. The bubbles are injected at position $x = 0$. The ultrasound frequency is 1 MHz and the acoustic pressure amplitude $P_A$ was set to have a Gaussian shape with a maximum amplitude of 4.5 kPa in the center of the channel (Fig. 1B). A microfluidic channel length $L$ of 1 cm was chosen. The aspect ratio $W/H$ was chosen to be 10 with a channel width $W$ of 200 $\mu$m resulting in a pressure drop $\Delta P$ of 20 kPa. The surface tension and density of water are used, $\sigma$ = 0.072 N/m and $\rho_l$ = 1000 kg/m$^3$, respectively. The polytropic gas constant was set to unity, $\gamma = 1$, as we use low driving pressure and isothermal behavior can be assumed in the gas core of the bubbles. The coupled equations are solved numerically in MATLAB by an ordinary differential equation solver `ode45`. The corresponding boundary conditions were $\dot{y}_b = 0$ and $\ddot{y}_b = 0$ at $t = 0$.

Figure 1C shows the modeled displacement in the y-

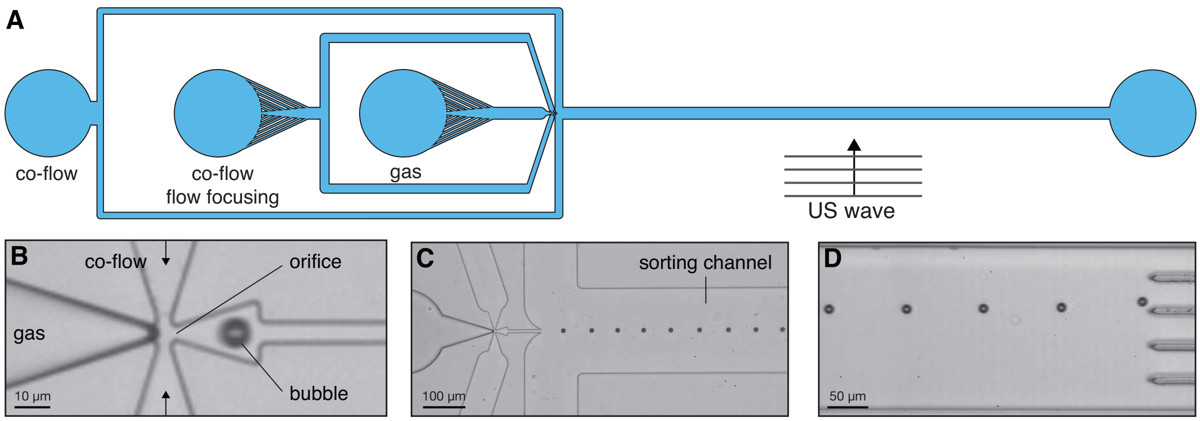


**Fig. 2** Acoustic bubble sorter. (A) shows the design of the experiments performed with the bubbles produced in a flow focusing device (B). Microbubbles are formed in a narrow orifice and directed into the sorting channel where an extra liquid co-flow is added to compensate for the bigger cross section (C). A traveling acoustic wave generated by an embedded piezo transducer displaces the bubbles over the channel width (D). Note: the channel lengths are not drawn to scale.

direction. We also plot the scattered pressure[39] of single microbubbles as a function of the bubble radius. The plot shows that the most resonant bubble sizes are displaced over the largest distance and that they can be separated from the other bubbles using the outlets of the sorting chip, see Fig. 1A. The output bubble size distribution can be controled by tuning the ultrasound frequency of the traveling wave. Shifting it towards higher frequencies will provide smaller bubble sizes in the output of the sorter and vice versa, lower ultrasound frequencies lead to an enriched suspension containing larger bubbles. The width of the size distribution at the outlet can be tuned by controling the amplitude of the ultrasound wave. A higher pressure amplitude results in a larger overall displacement for all bubbles, providing a wider size distribution and more bubbles at the outlet. Narrowing the output size distribution can be achieved by lowering the pressure amplitude resulting in an enriched suspension of highly resonant bubbles.

## 3 Acoustic bubble sorting: chip design

The chip designs are displayed in Figs. 2A and 3A. We use a chip bulk material with an acoustic impedance similar to that of water to prevent reflections at the channel walls, which results in bubbles being attracted to the walls. Moreover, the use of an acoustically homogeneous material prevents the build-up of standing waves. A PDMS-water interface has an acoustic reflection coefficient of only 20%[40], whereas for a glass-water or silicon-water interface nearly all the acoustic energy is reflected. We therefore build all sorting channels in PDMS.

The sorting channels (Fig. 2C) are straight large-aspect ratio channels with a piezo transducer embedded in the PDMS. The transducer generates a traveling acoustic wave perpendicular to the flow direction to push the bubbles to the top half of the channel. Outlet collection channels and chambers were not incorporated in the present design to avoid flow disturbances due to hydrodynamic pressure differences across the various outlets. Nevertheless, channel spacers were added to the sorting channel to mimic such outlets (Fig. 2D).

The molds for the PDMS chips were fabricated using standard soft lithography techniques[41]: a layer of SU-8 was spin-coated on top of a silicon wafer, UV-exposed through a mask containing the channel features, and developed to be ready for replica molding. PDMS was mixed in the standard $1:10$ ratio, degassed, poured over the mold and cured at 65°C for one hour, then cut to size. Prior to bonding, the fluidic ports were punched through the PDMS. The PDMS containing the channel features was plasma-bonded to a flat backing slab of PDMS for acoustic homogeneity. Teflon tubing (PEEK, Upchurch) was connected to the inlet channels through which gas, liquid, and ultrasound contrast agent were supplied. The outlets were connected to large diameter tubing to ensure atmospheric pressure at the outlet. The channels were filled with water immediately after bonding to maintain hydrophilicity.

The piezoelectric transducers are positioned such that they oscillate perpendicular to the sorting channel, in a slit cut though both PDMS layers parallel to the sorting channel at a distance of approximately 4.5 mm. They were glued using PDMS which was locally cured with a hot air gun. Three sizes of piezoelectric ceramics were used (surface area $5 \times 2$ mm$^2$, thickness 11 mm, $5 \times 5$ mm$^2$, thickness 2 mm, and $4 \times 4$ mm$^2$, thickness 1 mm) with center frequencies of 180 kHz, 1 MHz

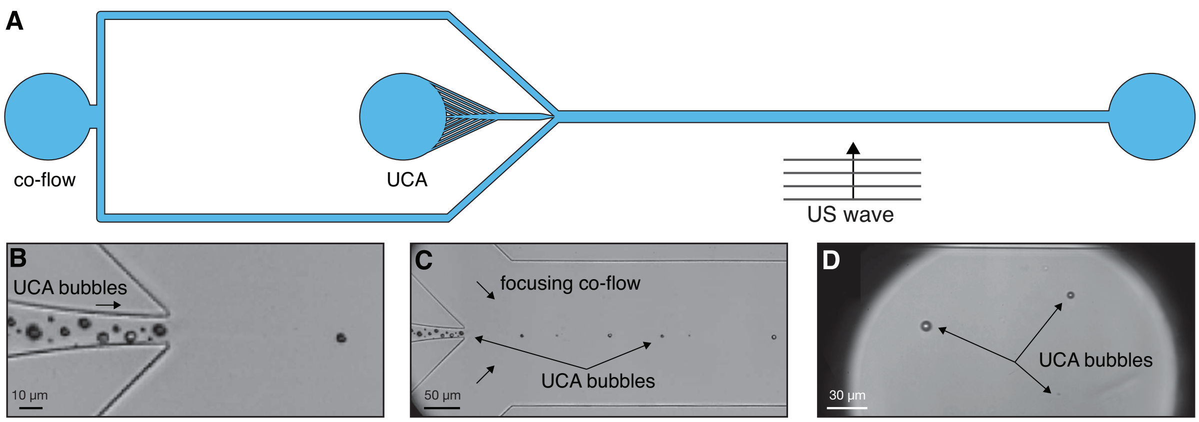


**Fig. 3** Acoustic bubble sorter for the sorting of UCAs. (A) shows the design. A microbubble suspension is hydrodynamically focused in between two liquid co-flows (B) forming a bubble train (C). A traveling acoustic wave pushes the bubbles in vertical direction downstream of the channel (D). Note: the channel lengths are not drawn to scale.

and 2 MHz, respectively. All transducers were driven at their thickness mode by an arbitrary waveform generator (Tabor Electronics, WW1072) operating in continuous mode. A sinusoidal waveform was applied with amplitudes of 2.4, 2.7, and 2.1 V, respectively. A quantitative measurement of the acoustic pressure on-chip using non-intrusive methods can be done through indirect radiation pressure measurements[42] or using Schlieren imaging[43]. However, these techniques are not applicable with the low acoustic pressure amplitudes used here. We subdivide the chip in two pieces, cut along the sorting channel, and we construct a watertight container around the part containing the piezo by positioning it between two glass slides and sealing it with PDMS, see Fig. 4. A calibrated hydrophone (Onda HNR-050) connected to an *x-y-z* translation stage was put in the water-filled container and moved along the sorting channel at a stand-off distance of approximately 0.2 mm. The piezo transducer was driven at the experimental conditions to estimate the applied pressure and the pressure distribution inside the sorting channel. It was verified that the water level above the channel did not influence the pressure measurements. Also the hydrophone did not suffer from electromagnetic interference and crosstalk from the piezo transducer.

The sorting strategy was first tested by connecting a flow focusing geometry[44] to the sorting channel (Fig. 2B). In the flow focusing geometry a gas thread is focused between two co-flows through a narrow orifice. Bubbles are produced sequentially to form a train of equally sized and equally spaced bubbles. The spacing between the bubbles is important to minimize the attractive forces between the bubbles which leads to bubble clustering. Two or more bubbles attached to each other have a completely different resonance behavior[32], which would render the proposed acoustic bubble sorting strategy impracticable. One can calculate that it is necessary to space the bubbles by a distance $d > 10R$[30].

Two flow focusing geometries were used to cover the gas and liquid flow rates to produce bubbles in the size range of interest, 1–25 $\mu$m. Bubbles with radii between 10 and 25 $\mu$m were produced in a flow focusing geometry with an orifice size of 20 $\mu$m, the smaller bubbles were produced with an orifice of 3 $\mu$m in size. Optically, the larger microbubbles are easier to measure and to size. The motivation for the smaller bubbles was to study the response of bubbles with a size similar

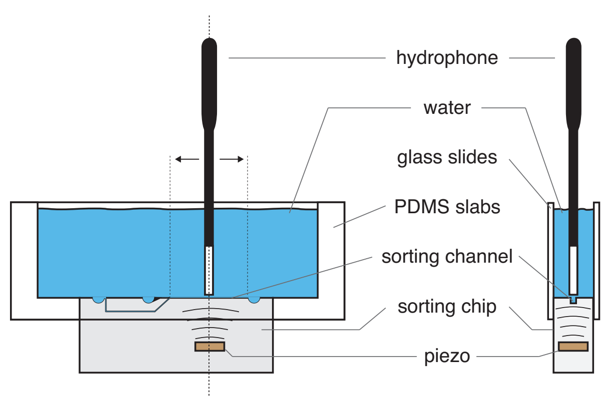


**Fig. 4** Pressure calibration setup. The sorting chip was cut in two halves along the sorting channel. A watertight container was constructed around the chip using two glass slides and a set of PDMS slabs. A calibrated hydrophone was moved along the channel axis to measure the acoustic pressure.

to those of UCA microbubbles. The sizing of these bubbles suffers from the effects of Mie scattering, in addition to that of optical diffraction.

The bubble size was varied by varying the gas pressure. Nitrogen gas flow is controled by a pressure regulator (Omega, PRG101-25) connected to a pressure sensor (Omega, DPG1000B-30G). Both liquid co-flows contain a surfactant to stabilize the bubbles and are comprised of a 5% w-w solution of dish washing liquid (Dreft, Procter and Gamble) in deionized water. The flow rate is controled by a high-precision syringe pump (Harvard Apparatus, PHD 2000, Holliston, MA, USA).

The outlets of the flow focusing geometries enter at the half width of the sorting channel for symmetry, a co-flow is added here to compensate for the bigger cross section. The sorting channels had a cross section of 113 $\times$ 500 $\mu$m$^2$ and 14 $\times$ 200 $\mu$m$^2$ for the larger and smaller flow focusing geometry, respectively. Both sorting channels had a total length of 1 cm. The height of the channels was the same throughout, flow focusing part and sorting channels alike. The flow rates for the flow focusing experiments with the larger bubbles were 35 $\mu$L/min for the flow-focusing and 1 mL/min for the confluent flow. For the smaller bubbles, the flow rates were 1 $\mu$L/min and 10 $\mu$L/min, respectively. All liquid and gas flows were filtered by an in-line syringe filter to prevent channel clogging by dust particles.

A perfluorobutane-based ultrasound contrast agent (Bracco BR-14, Bracco Research Geneva) was supplied in a 5 mL vial. The bubbles form a suspension once water is injected into the vial and the stabilizing shell is formed by a mixture of DSPC/DPPC phospholipids surrounded by a PEG emulsifier. The bubble suspension was focused between two co-flows (Fig. 3B) to form a train of bubbles with sufficiently large interbubble spacing and then injected into the sorting channel, as before (Fig. 3C). The cross section of the sorting channel was 14 $\times$ 200 $\mu$m$^2$. The syringe pump controlling the UCA flow was positioned vertically with the needle tip pointing upward at a level several tens of cms lower than the sorting chip. With the bubbles being buoyant, the aid of gravity helped inject the bubble suspension into the sorting chip. The contrast bubbles were infused at a rate of 4 $\mu$L/min and the liquid co-flow had a total flow rate of 24 $\mu$L/min.

The translation of the bubbles in the sorting channel was imaged using a high-speed camera (Photron SA1.1) connected to a microscope (Olympus BX-FM modular system) equipped with a water-immersion objective (Olympus, LUMPlanFL). A 20$\times$ magnification objective was used for the flow focusing experiment with the largest microbubbles, a 40$\times$ objective during the flow focusing experiment with the smaller bubbles and a 60$\times$ objective during the UCA sorting experiments. The obtained resolution was 1 $\mu$m, 0.5 $\mu$m, and 0.3 $\mu$m per pixel, respectively. The system was illuminated in transmitted light

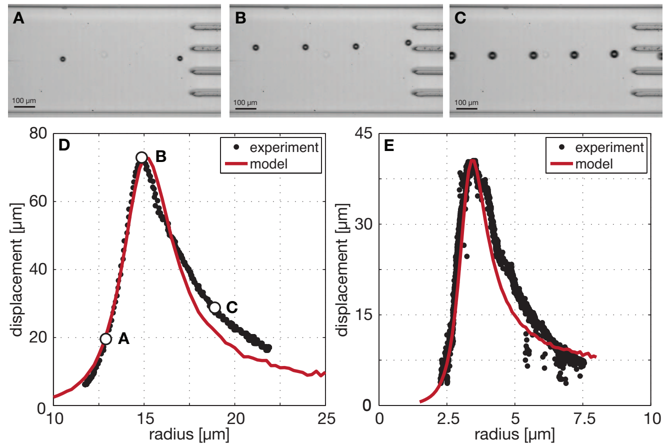


**Fig. 5** The acoustic bubble sorter in operation for bubbles produced in the flow focusing geometries. Bubbles with a resonance frequency higher (A) and bubbles with a resonance frequency lower (C) than the ultrasound frequency are displaced less than bubbles driven at resonance (B). Figure D shows the measured displacement as a function of the bubble radius (dots) for bubbles displaced in a 185 kHz wave. The solid red line shows the modeled displacement. Figure E shows the measured displacement as a function of bubble radius (dots) for bubbles displaced by a 1 MHz wave.

mode using fiber illumination (Olympus ILP-1) connected to a collimation objective (10$\times$ Olympus Plan Achromat 0.25 NA) positioned below the fluidic chip to maximize the light intensity at the imaging position. All high-speed recordings were captured at 5000 frames per second giving a temporal resolution of 0.2 ms and the shutter time was set to 16 $\mu$s to minimize motion blur.

The high-speed movies were processed frame by frame in MATLAB. First a background graylevel was subtracted from each frame, second the frame was converted to a binary image using a thresholding algorithm. From the binary image the center of the bubble was determined and it was used to transform the cartesian image $(x, y)$ into polar coordinates $(r, \theta)$. The intensity values of the original image were averaged over all $\theta$ angles to suppress noise in the intensity profile of the image of the bubble and to achieve a sub-pixel precision. The inflection point on the intensity profile was then taken as the radius of the bubble.

## 4 Results

Figure 5 shows the acoustic bubble sorter in operation. Figure 5A–C were taken from the high-speed recordings and show the displacement of the bubbles in the $y$-direction ($R$ = 13.2 $\mu$m, 15.0 $\mu$m, and 19.8 $\mu$m). The displacement of 566 bubbles normal to the direction of the channel flow is shown in Fig. 5D. The bubbles had a size range from 12 $\mu$m to 22 $\mu$m. The open dots indicate the displacement of the bubbles from the top figures.

The displacement curve shows the resonant behaviour of the bubbles. The solid red line in Fig. 5D represents the modeled displacement. Input to the model were the ultrasound frequency $f$ = 185 kHz, the speed of sound in water $c$ = 1490 m/s, the density of water $\rho$ = 1000 kg/m$^3$, and the measured pressure $P_A$. The pressure drop over the sorting channel $\Delta P$ = 5 kPa was calculated from the applied flow rate and was used in equation 5 as input to the local hydrodynamic pressure $P_0$, being the atmospheric pressure plus the channel pressure which decreases linearly with increasing $x$. The bubbles produced here were coated with a surfactant and in the model we set the surface tension to $\sigma$ = 0.03 N/m[14], and the surface tension of the gas-liquid interface was assumed not to vary with the bubble radius. The bubbles were also assumed to oscillate isothermally, therefore the polytropic gas constant was set to $\kappa = 1$.

Figure 5E shows the displacement of 1876 bubbles as a function of the bubble radius for the smaller flow focusing device. Here the bubbles range in size between 2.5 and 7.5 $\mu$m. The solid red line shows the modeled displacement using the measured acoustic pressure amplitude, as before. The pressure drop over the sorting channel was calculated to be $\Delta P$ = 100 kPa. The input parameters to the model are the ultrasound frequency $f$ = 1 MHz, the other input parameters, i.e. the speed of sound in water, the density of water and the surface tension of the surfactant interface, were taken as before.

Figure 6 shows the scatter plot of the displacement of 481 BR-14 UCA microbubbles by a 2 MHz traveling ultrasound wave. The displacement was measured 7 mm downstream of the entrance of the sorting channel. The size range is between 0.5 $\mu$m and 10 $\mu$m, and corresponds to the typical size distribution of BR-14. The typical acoustic pressure used here was 15 kPa. Extensive research on the dynamical behavior of ultrasound contrast agents has been performed in the past[45–47]. More recently it came to the attention that the nonlinear harmonic response of UCA is governed, not only by the classical Rayleigh-Plesset-type nonlinear bubble dynamics, but to a great extent also by the nonlinear properties of the bubble shell[48,49]. It was also shown that the shell surfactant concentration had a major impact on the generation of the harmonic response, i.e. even for bubbles of the same size a very different acoustic response can be observed[50,51]. The bubbles can oscillate in an elastic regime with a low concentration of phospholipids and finite surface tension, or they can oscillate in a buckled regime owing to the high concentration of phospholipids with virtually no surface tension[48]. The viscoelastic properties of the phospholipid shell of BR-14 contrast bubbles can be incorporated into the bubble dynamics equation, Eq. (3), by adding pressure contributions for an effective shell

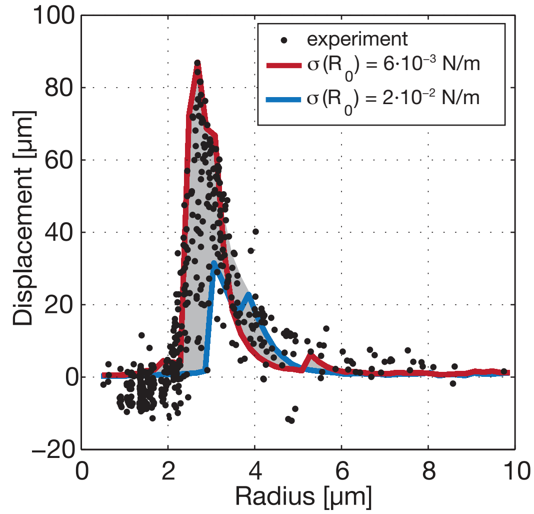


**Fig. 6** Experimentally obtained displacement of UCA bubbles as a function of the bubble size (dots). The red line shows the modeled displacement of coated bubbles with an initial surface tension of $6\times10^{-3}$ N/m and the blue line shows the modeled displacement for a initial surface tension of $2\times10^{-3}$ N/m. Varying the initial surface tension between these two values (gray area) show excellent agreement with the measured displacement.

elasticity and rate-dependent shell viscosity. The varying shell surfactant concentration is captured in a parameter termed the initial surface tension $\sigma(R_0)$[50]. To induce the flow the pressure drop over the sorting channel was approximately 100 kPa. Such a large overpressure may compress the contrast bubbles, which results in bubbles ending up in their buckled state, or at least close to buckling, with an initial surface tension close to zero.

Numerical simulations of the displacement were performed using the measured acoustic pressure amplitude and the data for BR-14 bubbles from Overvelde *et al.*[52]. They showed that BR-14 bubbles are characterized by a shell elasticity of 2.5 N/m together with a shell viscosity of $6.0 \times 10^{-9}$ kg/s. The initial surface tension $\sigma(R_0)$ of contrast microbubbles in their suspension varied between zero and 0.035 N/m. A polytropic gas constant of $\kappa = 1.07$ for perfluorobutane ($C_4F_{10}$) gas was used and all properties of the surrounding liquid were kept as before. Figure 6 shows the modeled displacement of bubbles with an initial surface tension between $6 \times 10^{-3}$ N/m (in red) and $2 \times 10^{-2}$ N/m (in blue). The gray area fills all possible displacement curves between the two extremes and we find very good agreement with the measured results.

## 5 Discussion

Typically one to ten billion bubbles are injected in a human perfusion study. Injecting an enriched bubble suspension with a narrow size distribution may dramatically decrease the number of bubbles that is needed during such an imaging procedure, a decrease of 20–40 times is expected in favorable conditions. Still, with the single sorting channel, operated under the conditions as described here, it would take several hours to fill a vial with millions of resonant bubbles. Massive parallelization of the sorting method may be achieved by stacking microfluidic channel layers in close proximity to each other[53], which will then reduce the sorting time to under one minute.

Flow focusing techniques are capable of producing up to $10^6$ bubbles per second from a single orifice[15]. While flow focusing techniques have an excellent track record in producing highly monodisperse bubble suspensions, also for coated bubbles, with a polydispersity index down to 0.2%, there is very little knowledge on the details of the coating characteristics and on the dynamic process of coating during formation. Thus, it can be very helpful, even for monodisperse bubble production facilities, to sort the suspension of bubbles in a subsequent step based on their acoustic property, not necessarily on size.

In preclinical small animal models, only a small amount of bubbles can be safely injected. For these protocols it is therefore of great importance to inject only those bubbles that are acoustically most responsive. Hence it would be beneficial to use sorted bubbles with high echogenicity instead of a polydisperse suspension containing a large fraction of smaller and larger non-resonant bubbles. This feature becomes even more important when using the contrast bubbles in harmonic imaging as all nonlinear harmonic behavior is concentrated near resonance. Thus, the injection of non-responsive larger bubbles will primarily contribute to a substantial scattering echo at the fundamental frequency and to attenuation of the transmit signal, thereby limiting the scattering to attenuation ratio (STAR) of the nonlinear echo. Acoustic bubble sorting is also beneficial for targeted bubbles for molecular imaging and to sort drug and gene loaded bubbles. The bubbles passing the bubble sorter at the waste outlet may be reinjected in another chip to be sorted at a different frequency for use in another treatment. Finally, the expensive drug load and/or targeting ligands may also be recycled from the waste collection channel.

A few words on the modeling efforts are in order. We have added a linear damping term to the Rayleigh-Plesset model to account for the energy dissipation of the radial oscillations. These arise first of all from the presence of a surfactant layer to stabilize the bubbles produced in the flow focusing geometry and secondly from the interaction of the bubbles with the PDMS walls. Finally, we know from Devin[54] that thermal damping of bubbles with a size near 15 $\mu$m are dominant over the other damping contributions, such as acoustic reradiation and viscous dissipation. To cover all these (unknown) damping contributions we introduced a single damping factor $\delta_{\text{add}}$ as a pressure contribution in the form $-\delta_{\text{add}}\rho_l\omega R\dot{R}$ as in Eatock *et al.*[55]. The width of the modeled displacement curves in Fig. 5 were fitted to the measured displacement curves by varying $\delta_{\text{add}}$. We find a total damping of 0.24 and 0.40 for the 15 $\mu$m and 3 $\mu$m bubbles, respectively. The total damping and the maximum displacement are highly coupled. Moreover, the modeled displacement strongly depends on the input acoustic pressure amplitude which was measured using an intrusive technique with a potential bias in both its amplitude and position. The combination of all these factors led us to scale the modeled displacement in figures 5D and E to the experimental data with a scaling factor of 1.7 and 1.4, respectively, while keeping good agreement in the overall shape of the displacement curve. For the contrast agent microbubbles we incorporate the visco-elastic shell parameters (shell elasticity, shell viscosity and surfactant concentration) directly from experimental microbubble characterization studies[52] and we find good agreement for the displacement curves and its sorting capabilities.

The microbubbles in our sorting channels are always close to the PDMS walls of the chip. There is a large inconsistency between the available theoretical models that describe the dynamics of microbubbles close to a compliant wall. Doikinov *et al.*[56] model the dynamics of contrast agent microbubbles near a polystyrene Opticell® membrane and their model predicts an increase of the resonance frequency for a bubble close to the wall. Hay *et al.*[57] find a decrease of the resonance frequency for a bubble between two viscoelastic layers. Recent experiments by Helfield *et al.*[58] show very different acoustical behavior for bubbles close to an agar wall (with a small difference in acoustic impedance, hence little change in the bubble dynamics) as compared to an Opticell membrane with considerably larger changes. The acoustic transparency of PDMS suggests a minor influence of the bubble-wall interaction with limited change to the dynamics of the bubbles. Experiments of single microbubbles with a given stand-off distance to a PDMS wall or between two PDMS walls, e.g. using optical tweezers[59], should clarify the details of bubble-wall interactions relevant for our sorting chip.

## Conclusions

We have demonstrated a simple lab-on-a-chip device to sort coated microbubbles on-line in a travelling acoustic wave. The bubbles are sorted to their acoustic property rather than to their size, which makes the proposed sorting strategy highly efficient for injection of a smaller dose, yet highly resonant, enriched bubble suspension for preclinical small animal imaging, for targeted molecular imaging using ultrasound, and for drug and gene delivery applications.


## Acknowledgments

We acknowledge the help of Stefan Schlautmann in producing the soft-lithography molds and for assistance and training in the clean room facilities of MESA$^+$. We also thank David Fernandez-Rivas for sharing his insightful experimental experience in microfluidic fabrication technology. We thank Wim van Hoeve, Peter Frinking, Nico de Jong, and Detlef Lohse for stimulating discussions. We also want to thank Gert-Wim Bruggert, Martin Bos, and Bas Benschop for their skilful technical assistance. We thank Bracco Research Geneva for the supply of BR-14 ultrasound contrast agents. This work is supported by NanoNextNL, a micro and nanotechnology consortium of the Government of the Netherlands and 130 partners.


## References


1 N. de Jong, F. ten Cate, C. Lancée, J. Roelandt, and N. Bom, “Principles and recent developments in ultrasound contrast agents”, Ultrasonics **29**, 324–330 (1991).

2 J. R. Lindner, “Microbubbles in medical imaging: current applications and future directions”, Nature Reviews Drug Discovery **3**, 527–533 (2004).

3 A. L. Klibanov, “Microbubble Contrast Agents: Targeted ultrasound imaging and ultrasound-assisted drug-delivery applications.”, Invest. Radiol. **41**, 354–362 (2006).

4 J. Tsutsui, F. Xie, and R. Porter, “The use of microbubbles to target drug delivery”, Cardiovasc Ultrasound **2**, 23 (2004).

5 S. Hernot and A. L. Klibanov, “Microbubbles in ultrasound-triggered drug and gene delivery ”, Adv. Drug Deliv. Rev. **60**, 1153–1166 (2008).

6 L. Deelman, A. Declèves, J. Rychak, and K. Sharma, “Targeted renal therapies through microbubbles and ultrasound”, Adv. Drug Deliv. Rev. **62**, 1369–1377 (2010).

7 A. Carson, C. McTiernan, L. Lavery, M. Grata, X. Leng, J. Wang, X. Chen, and F. Villanueva, “Ultrasound-targeted microbubble destruction to deliver siRNA cancer therapy”, Cancer Res. **72**, 6191–6199 (2012).

8 M. Minnaert, “On musical air-bubbles and the sound of running water”, Philosophical Magazine **16**, 235–248 (1933).

9 E. Talu, K. Hettiarachchi, S. Zhao, R. L. Powell, A. P. Lee, L. Longo, and P. A. Dayton, “Tailoring the size distribution of ultrasound contrast agents: Possible Method for Improving Sensitivity in Molecular Imaging”, Mol. Imaging **6**, 384–392 (2007).

10 M. Overvelde, V. Garbin, B. Dollet, N. de Jong, D. Lohse, and M. Versluis, “Dynamics of coated microbubbles adherent to a wall”, Ultrasound Med. Biol. **37**, 1500–1508 (2011).

11 A. M. Gañán-Calvo and J. M. Gordillo, “Perfectly monodisperse microbubbling by capillary flow focusing”, Phys. Rev. Lett. **87**, 274501 (2001).

12 S. L. Anna, N. Bontoux, and H. A. Stone, “Formation of dispersions using ”flow focusing” in microchannels”, Appl. Phys. Lett. **82**, 364–366 (2003).

13 P. Garstecki, H. Stone, and G. M. Whitesides, “Mechanism for Flow-Rate Controlled Breakup in Confined Geometries: A Route to Monodisperse Emulsions”, Phys. Rev. Lett. **94**, 164501 (2005).

14 B. Dollet, W. van Hoeve, J.-P. Raven, P. Marmottant, and M. Versluis, “Role of the Channel Geometry on the Bubble Pinch-Off in Flow-Focusing Devices”, Phys. Rev. Lett. **100**, 034504 (2008).

15 K. Hettiarachchi, E. Talu, M. L. Longo, A. Dayton, and A. P. Lee, “On-chip generation of microbubbles as a practical technology for manufacturing contrast agents for ultrasonic imaging”, Lab. Chip **7**, 463–468 (2007).

16 E. Talu, K. Hettiarachchi, R. L. Powell, A. P. Lee, P. A. Dayton, and M. L. Longo, “Maintaining monodispersity in a microbubble population formed by flow-focusing”, Langmuir **24**, 1745–1749 (2008).

17 J. Kwan and M. Borden, “Lipid monolayer mechanics during microbubble gas exchange”, Soft Matter **8**, 4756–4766 (2012).

18 R. Shih, D. Bardin, T. D. Martz, P. S. Sheeran, P. A. Dayton, and A. P. Lee, “Flow-focusing regimes for accelerated production of monodisperse drug-loadable microbubbles toward clinical-scale applications”, Lab. Chip **13**, 4816–4826 (2013).

19 J. Streeter, R. Gessner, I. Miles, and P. Dayton, “Improving sensitivity in ultrasound molecular imaging by tailoring contrast agent size distribution: in vivo studies”, Mol. Imaging **9**, 87–95 (2010).

20 M. Emmer, A. van Wamel, D. E. Goertz, and N. de Jong, “The onset of microbubble vibration”, Ultrasound Med. Biol. **33**, 941–949 (2007).

21 D. E. Goertz, N. de Jong, and A. F. W. van der Steen, “Attenuation and size distribution measurements of Definity and manipulated Definity populations.”, Ultrasound Med. Biol. **33**, 1376–1388 (2007).

22 J. A. Feshitan, C. C. Chen, J. J. Kwan, and M. A. Borden, “Microbubble size isolation by differential centrifugation.”, J. Coll. Interf. Sci **329**, 316–324 (2009).

23 H. A. Nieuwstadt, R. Seda, D. S. Li, J. B. Fowlkes, and J. L. Bull, “Microfluidic particle sorting utilizing inertial lift force”, Biomedical Microdevices **13**, 97–105 (2010).

24 M. Yamada, M. Nakashima, and M. Seki, “Pinched Flow Fractionation: Continuous Size Separation of Particles Utilizing a Laminar Flow Profile in a Pinched Microchannel”, Anal. Chem. **76**, 5465–5471 (2004).

25 M. Hill and N. R. Harris, “Ultrasonic particle manipulation”, in *Microfluidic Technologies for Miniaturized Analysis Systems*, 357–383 (Springer-Verlag, New York) (2007).

26 T. Laurell, F. Petersson, and A. Nilsson, “Chip integrated strategies for acoustic separation and manipulation of cells and particles”, Chemical Society Reviews **36**, 492–506 (2007).

27 I. González, L. J. Fernández, T. E. Gómez, J. Berganzo, J. L. Soto, and A. Carrato, “A polymeric chip for micromanipulation and particle sorting by ultrasounds based on a multilayer configuration”, Sensors and Actuators B: Chemical **144**, 310–317 (2010).

28 P. Thevoz, J. D. Adams, H. Shea, H. Bruus, and H. T. Soh, “Acoustophoretic synchronization of mammalian cells in microchannels”, Anal. Chem. **82**, 3094–3098 (2010).

29 V. F. K. Bjerknes, “Fields of Force”, Columbio University Press, New York 1–136 (1906).

30 L. A. Crum, “Bjerknes forces on bubbles in a stationary sound field”, J. Acoust. Soc. Am. **57**, 1363–1370 (1957).

31 P. Marmottant, M. Versluis, N. de Jong, S. Hilgenfeldt, and D. Lohse, “High-speed imaging of an ultrasound-driven bubble in contact with a wall: Narcissus effect and resolved acoustic streaming”, Exp. Fluids **41**, 147–153 (2006).

32 T. Leighton, *The Acoustic Bubble* (Academic Press) (1994).

33 T. Watanabe and Y. Kukita, “Translational and radial motions of a bubble in an acoustic standing wave field”, Phys. Fluids **5**, 2682–2688 (1993).

34 S. Zhao, M. Borden, S. H. Bloch, D. Kruse, K. W. Ferrara, and P. A. Dayton, “Radiation-force assisted targeting facilitates ultrasonic molecular imaging”, Phys. Fluids **3**, 135–148 (2004).

35 V. Garbin, B. Dollet, M. Overvelde, D. Cojoc, E. di Fabrizio, L. van Wijngaarden, A. Prosperetti, N. de Jong, D. Lohse, and M. Versluis, “History force on coated microbubbles propelled by ultrasound”, Phys. Fluids **21**, 092003 (2009).

36 L. Landau and E. M. Lifschitz, *Fluid Mechanics*, 2nd edition (Pergamon,

New York) (1987).

37 J. Magnaudet and I. Eames, "The motion of high-Reynolds-number bubbles in inhomogeneous flows", Ann. Rev. Fluid Mech. **32**, 659–708 (2000).

38 H. Bruus, *Theoretical Microfluidics* (Oxford University Press) (2008).

39 K. Vokurka, "On Rayleigh's model of a freely oscillating bubble. 1. Basic relations", Czechoslovak Journal of Physics **35**, 28–40 (1985).

40 K. Zell, J. I. Sperl, M. W. Vogel, R. Niessner, and C. Haisch, "Acoustical properties of selected tissue phantom materials for ultrasound imaging", Phys. Med. Biol. **52**, 475–484 (2007).

41 D. C. Duffy, J. C. McDonald, O. J. A. Schueller, and G. M. Whitesides, "Rapid prototyping of microfluidic systems in poly(dimethylsiloxane)", Anal. Chem. **70**, 211–217 (1998).

42 R. Barnkob, P. Augustsson, T. Laurell, and H. Bruus, "Measuring the local pressure amplitude in microchannel acoustophoresis", Lab. Chip **10**, 563–570 (2010).

43 R. T. Held, V. Zderic, T. N. Nguyen, and S. Vaezy, "Annular phased-array high-intensity focused ultrasound device for image-guided therapy of uterine fibroids", IEEE Transaction on ultrasonics, ferroelectrics, and frequency control **53**, 335–348 (2006).

44 Y.-C. Tan, V. Cristini, and A. P. Lee, "Monodispersed microfluidic droplet generation by shear focusing microfluidic device", Sensors and Actuators B: Chemical **114**, 350–356 (2006).

45 N. de Jong, R. Cornet, and C. Lancée, "Higher harmonics of vibration gas-filled microspheres. part one: simulations", Ultrasonics **32**, 447 (1994).

46 C. C. Church, "The effect of an elastic solid surface layer on the radial pulsation of gas bubbles", J. Acoust. Soc. Am. **97**, 1510 – 1521 (1995).

47 L. Hoff, P. Sontum, and J. Hovem, "Oscillations of polymeric microbubbles: Effect of the encapsulating shell", JASA **107**, 2272–2280 (2000).

48 P. Marmottant, S. Van Der Meer, M. Emmer, M. Versluis, N. De Jong, S. Hilgenfeldt, and D. Lohse, "A model for large amplitude oscillations of coated bubbles accounting for buckling and rupture", J. Acoust. Soc. Am. **118**, 3499 – 3505 (2005).

49 K. Sarkar, W. T. Shi, D. Chatterjee, and F. Forsberg, "Characterization of ultrasound contrast microbubbles using in vitro experiments and viscous and viscoelastic interface models for encapsulation", J. Acoust. Soc. Am. **118**, 539 – 550 (2005).

50 J. Sijl, B. Dollet, M. Overvelde, V. Garbin, T. Rozendal, N. de Jong, D. Lohse, and M. Versluis, "Subharmonic behavior of phospholipid-coated ultrasound contrast agent microbubbles", J. Acoust. Soc. Am. **128**, 3239–3252 (2010).

51 J. Sijl, M. Overvelde, B. Dollet, V. Garbin, N. de Jong, D. Lohse, and M. Versluis, ""Compression-only" behavior: A second-order nonlinear response of ultrasound contrast agent microbubbles", J. Acoust. Soc. Am. **129**, 1729–1739 (2011).

52 M. Overvelde, V. Garbin, J. Sijl, B. Dollet, N. de Jong, D. Lohse, and M. Versluis, "Nonlinear shell behavior of phospholipid-coated microbubbles.", Ultrasound Med. Biol. **36**, 2080–2092 (2010).

53 M. Hashimoto, S. S. Shevkoplyas, B. Zasońska, T. Szymborski, P. Garstecki, and G. M. Whitesides, "Formation of bubbles and droplets in parallel, coupled flow-focusing geometries", Small **4**, 1795–1805 (2008).

54 C. Devin, "Survey of Thermal, Radiation, and ViscousDamping of Pulsating Air Bubbles in Water", J. Acoust. Soc. Am. **31**, 1654–1667 (1959).

55 B. C. Eatock, R. Y. Nishi, and G. W. Johnston, "Numerical studies of the spectrum of low-intensity ultrasound scattered by bubbles", J. Acoust. Soc. Am. **77**, 1692–1701 (1985).

56 A. A. Doinikov, L. Aired, and A. Bouakaz, "Dynamics of a contrast agent microbubble attached to an elastic wall.", IEEE Trans. Med. Imaging **31**, 654–662 (2012).

57 T. A. Hay, Y. A. Ilinskii, E. A. Zabolotskaya, and M. F. Hamilton, "Model for bubble pulsation in liquid between parallel viscoelastic layers.", J. Acoust. Soc. Am. **132**, 124–137 (2012).

58 B. L. Helfield and D. E. Goertz, "Nonlinear resonance behavior and linear shell estimates for Definity and MicroMarker assessed with acoustic microbubble spectroscopy", J. Acoust. Soc. Am. **133**, 1158–1168 (2013).

59 V. Garbin, D. Cojoc, E. Ferrari, E. Di Fabrizio, M. L. J. Overvelde, S. M. Van Der Meer, N. De Jong, D. Lohse, and M. Versluis, "Changes in microbubble dynamics near a boundary revealed by combined optical micromanipulation and high-speed imaging", Appl. Phys. Lett. **90**, 114103–3 (2007).



 